

Characteristics of the immune environment in prostate cancer as an adjunct to immunotherapy

Xinhai Yin¹ | Yadong Wu² | Jukun Song² 

¹Department of Oral and Maxillofacial Surgery, Guizhou Provincial People's Hospital, Guiyang, China

²Department of Oral and Maxillofacial Surgery, the Affiliated Stomatological Hospital of Guizhou Medical University, Guiyang, China

Correspondence

Jukun Song, Department of Oral and Maxillofacial Surgery, the Affiliated Stomatological Hospital of Guizhou Medical University, Guiyang 550002, China.
Email: songjukun@163.com

Abstract

Background and Aims: The tumor microenvironment (TME) exerts an important role in carcinogenesis and progression. Several investigations have suggested that immune cell infiltration (ICI) is of high prognostic importance for tumor progression and patient survival in many tumors, particularly prostate cancer. The pattern of immune infiltration of PCa, on the other hand, has not been thoroughly understood.

Methods: The Cancer Genome Atlas (TCGA) and the Gene Expression Omnibus (GEO) datasets on PCa were obtained, and several datasets were merged into one data set using the “ComBat” algorithm. The ICI profiles of PCa patients were then to be uncovered by two computer techniques. The unsupervised clustering method was utilized to identify three ICI patterns in tumor samples, and Principal Component Analysis (PCA) was conducted to estimate the ICI score.

Results: Three different clusters of three ICIs were identified in 1341 PCa samples, which also correlated with different clinical features/characteristics and biological pathways. Patients with PCa are classified into high and low subtypes based on the ICI scores extracted from immune-associated signature genes. High ICI score subtypes are associated with a worse prognosis, which may intrigue the activation of cancer-related and immune-related pathways such as pathways involving Toll-like receptors, T-cell receptors, JAK-STAT, and natural killer cells. The ICI score was linked to tumor mutation load and immune/cancer-relevant signaling pathways, which explain prostate cancer's poor prognosis.

Conclusion: The findings of this study not only advanced our knowledge of the mechanism of immune response in the prostate tumor microenvironment but also provided a novel biomarker, that is, the ICI score, for disease prognosis and guiding precision immunotherapy.

KEYWORDS

immune cell infiltration, principal component analysis, prostate cancer, tumor microenvironment

This is an open access article under the terms of the [Creative Commons Attribution-NonCommercial](https://creativecommons.org/licenses/by-nc/4.0/) License, which permits use, distribution and reproduction in any medium, provided the original work is properly cited and is not used for commercial purposes.

© 2024 The Author(s). *Health Science Reports* published by Wiley Periodicals LLC.

1 | INTRODUCTION

Prostate cancer remains one of the leading worldwide health concerns in males. Each year, over 230,000 new instances of prostate cancer are discovered in the US, and about 195,000 radical prostatectomy procedures are carried out.^{1,2} According to the latest data from the American Cancer Society (ACS), the relative survival rates for prostate cancer patients at 5, 10, and 15 years are 99%, 98%, and 96% respectively. The percentage of men without prostate cancer in the overall population.³ These data indicate that the extensive majority of new presentations are with locally advanced diseases, representing significant healthcare and substantial economic burdens. Up to 35% of men who have radical prostatectomy will develop PSA recurrence within 10 years of surgery, which is often brought on by micro-metastatic disease after surgery, even though early detection gives the chance for curative treatment.⁴⁻⁶ Recent advancements in the treatment of prostate cancer have significant implications for both non-metastatic and metastatic settings. In patients with high-risk, non-metastatic prostate cancer, the combination of abiraterone and prednisolone with androgen deprivation therapy (ADT) is emerging as a new standard treatment. This therapeutic approach is supported by robust clinical evidence indicating its efficacy in prolonging survival without progression of the disease.⁷ In contrast, for patients with metastatic prostate cancer initiating long-term ADT, the concurrent use of enzalutamide and abiraterone is not recommended. Studies have shown that while each agent separately enhances the effectiveness of ADT, their combination does not yield additional benefits and may increase the risk of adverse effects.⁷ Furthermore, the addition of abiraterone to ADT has been demonstrated to maintain clinically significant improvements in survival for a duration extending beyond 7 years, highlighting its long-term benefits in managing prostate cancer.⁷ Currently, molecular marker profiles have been established to differentiate between aggressive and indolent forms of prostate cancer (PCa). However, there remains a significant need to identify new and improved predictive markers to increase the precision of diagnostic predictions. Urinary liquid biopsies, which are noninvasive and enriched with specific biomarkers, offer a promising avenue for detection. Additionally, immune cell infiltrates in tumors, comprising B-lymphocytes, T-lymphocytes, dendritic cells, macrophages, granulocytes, monocytes, and various polarized immune cells, have the potential to influence cancer progression. Bone sialoprotein (BSP) is associated with accelerated development of bone metastases, whereas osteopontin (OPN) is useful for monitoring chemotherapy responses in castration-resistant prostate cancer (CRPC). Moreover, certain microRNAs, such as miRNA-375, linked to lymph node involvement and metastasis, miRNA-141, essential for epithelial-to-mesenchymal transition, and miRNA-21, associated with disease pathogenesis and castration resistance, highlight the utility of these biomarkers. Serum microRNAs from the miRNA-200 and miRNA-17 families have been shown to correlate with prostate-specific antigen (PSA) response and overall survival in CRPC patients treated with docetaxel.⁸

Multiple works have demonstrated that immune cell infiltration (ICI) is crucial to the prognosis of various solid tumors.⁹⁻¹¹ The immune system has an excellent ability to recognize and kill potentially harmful cells (such as infected cells or cancer cells) that enter the body. However, in most tumor patients in progress, the antitumor immune response has never occurred or has been shut down by cancer. One effective way to combat tumors is to activate the patient's defense system through immunotherapy,^{12,13} but most immunotherapies based on specific T cell receptors (TCRs) only benefit subgroups of patients.^{14,15} Immune cell infiltration (ICI), one of the leading players in the tumor microenvironment (TME), participates in tumorigenic progression in multiple tumors; the profiles of ICI-involved genes can be leveraged to predict outcomes of cancer patients and guide neoadjuvant immunotherapies.⁹⁻¹¹ However, the ICI landscape in prostate cancer has yet been not completely understood. In the present study, the ICI genes of 1341 patient samples from six public datasets were obtained to derive a comprehensive outlook on immune response patterns in prostate cancer.

2 | MATERIAL AND METHODS

2.1 | Data set

Six accessible databases (GSE54460,¹⁶ GSE107299,¹⁷ GSE116918,¹⁸ Taylor (GSE21034),¹⁹ DKFZ2018,²⁰ our PCa cohort,²¹ and TCGA-prostate cancer) were included in the study. Among the datasets, RNA-sequence data (Fragments Per Kilo-base Million [FPKM] values) of PCa data set were sourced from the TCGA website (<https://portal.gdc.cancer.gov/>), GSE54460, GSE107299, GSE116918, Taylor's data were obtained from Gene Expression Omnibus (GEO) using the R package GEOquery.²² The DKFZ2018 was obtained from cBioPortal (<https://www.cbioportal.org/>).²³ The meta-GEO data were merged to eliminate the batch effect using the "ComBat" algorithm (Figure S1A and B).²⁴ GSE54460, GSE107299, GSE116918, GSE21034, DKFZ2018, and TCGA-prostate cancer were considered as the training set, while our PCa cohort was regarded as the testing set. Among these datasets, progression-free interval event (PFI) data for TCGA PCa and GSE70768, GSE116918, and Taylor were available in these four datasets.

2.2 | Unsupervised clustering analysis using a consensus algorithm

Using the "CIBERSORT" R package, LM22 immune cell sets, and 1,000 alignments, we estimated the relative infiltration fraction of immune cells in PCa.²⁵ To assess the immune and matrix composition of each PC sample (immune and matrix scores), an estimated approach was used.²⁶ Using an unsupervised hierarchical method, we grouped the PCa samples following each sample's ICI pattern. The "Pam" approach using Euclidean and Ward linkage was utilized in

this study, which was done using the “ConsensuClusterPlus” R package.²⁷

2.3 | Differentially expressed analysis among these ICI subgroups

Based on the invasion of immune cells, patients are classified into ICI clusters and genes linked to the ICI phenotype are identified. To identify differentially expressed genes (DEGs) in ICI subtypes, we carried out differentially expressed analysis using the criteria of a P-value of lower than 0.05 (after adjustment) and an absolute fold change of beyond 0.5, which was achieved by using the “Limma” R package.²⁸

2.4 | Establishment of ICI score

The expression levels of DEGs were utilized in conjunction with unsupervised clustering to categorize patients in the TCGA data set. Additionally, gene features A and B were assigned to the DEGs that were favorably and negatively linked with the gene cluster characteristics,²⁹ respectively. The dimension of gene signatures A and B was then minimized using Boruta's technique, and PCA was utilized to acquire PC I as a feature score. Ultimately, the ICI score for each patient was determined using a method identical to that used to calculate the Gene Expression Ranking Index.

$$\text{ICI score} = \sum \text{PCIA} + \sum \text{PCIB}$$

2.5 | Genomic alteration data

The mutation data of the TCGA-PCa cohort were obtained from the TCGA data set (<https://www.cancer.gov/tga/>). Tumor Mutational Burden (TMB) was calculated based on the overall count of mutations that result in amino acid changes in PCa. We used the “oncoplot” function of the ComplexHeatmap package to compare

somatic changes in PCa driver genes with high and low ICI scores.³⁰ Twenty-five of the most frequently mutated genes were shown.

3 | RESULTS

3.1 | Landscape of immune cell infiltration in PCa

To begin, the relative fraction of immune cells in PCa tumor tissues was quantified using the CIBERSORT and ESTIMATE methods on a meta-cohort of 1341 tumor samples in immune cells infiltration (ICI) profiles (DKFZ2018, GSE21034, GSE54460, GSE107299, GSE116918, and TCGA-PCa cohort) (Table 1). Secondly, the “ConsensusClusterPlus” package of R software was used to classify PCa patients into three groups based on a random clustering analysis. One thousand, three hundred forty-one PCa patients were unsupervised consensus clustered into 0 to 8 clusters. The change in the cumulative distribution function curve area in proportion to its initial value shows that starting from three clusters, the sample is almost completely stably distributed (Figure S2A and B).

The CIBERSORT program comprehensively compared the profiles of TME cell infiltration patterns across the three ICI clusters (Figure 1A). Significant variations in PFI survival were observed across three distinct ICI subtypes (log-rank test, $p = 0.039$; Figure 1B), but not for OS, DFI, and DSS (Figure 1C–E). To show the predominance of immune cell contacts in TME, we also construct correlation matrix heat maps (Figure 1F). We examined the immune cell makeup of the tumor environment to further clarify the inherent biological variations that result in various clinical presentations. ICI cluster A is distinguished by extremely naïve B cells, T cells CD8, T cells follicular helper, T cells regulatory (Tregs), active NK cells, Monocytes, M0 macrophages, and resting Mast cells. T cells CD4 memory resting, M1 and M2 macrophages, Dendritic cells resting, Stromal score, and immunological score were substantially greater in patients in ICI group B. Plasma cell infiltration was increased in ICI cluster C subjects (Figure 1G).

TABLE 1 Information of the six publicly available datasets.

Data set	Country	Number of samples	Transcriptome platform	Number of rows per platform	Tissue
TCGA PCa	USA	52 N, 499 T	Illumina HiSeq	60484	Fresh frozen
DKFZ2018	USA	118 T	Illumina HiSeq. 2000	20871	Fresh frozen
Taylor(GSE21034)	USA	29 N, 150 T	Affymetrix Human Exon 1.0 ST Array	45288	Fresh frozen
GSE54460	USA	107 T	Illumina HiSeq. 2000	60656	FFPE
GSE107299	Canada	213 T	Affymetrix Human Transcriptome Array 2.0	23935	Fresh frozen
GSE116918	United Kingdom	248 T	Almac Diagnostics Prostate Disease Specific Array	21162	FFPE

Abbreviations: FFPE, Formalin-fixed Paraffin embedded tissue blocks; GSE, Gene Expression Omnibus Series; N, paracancerous normal samples; T, tumor samples.

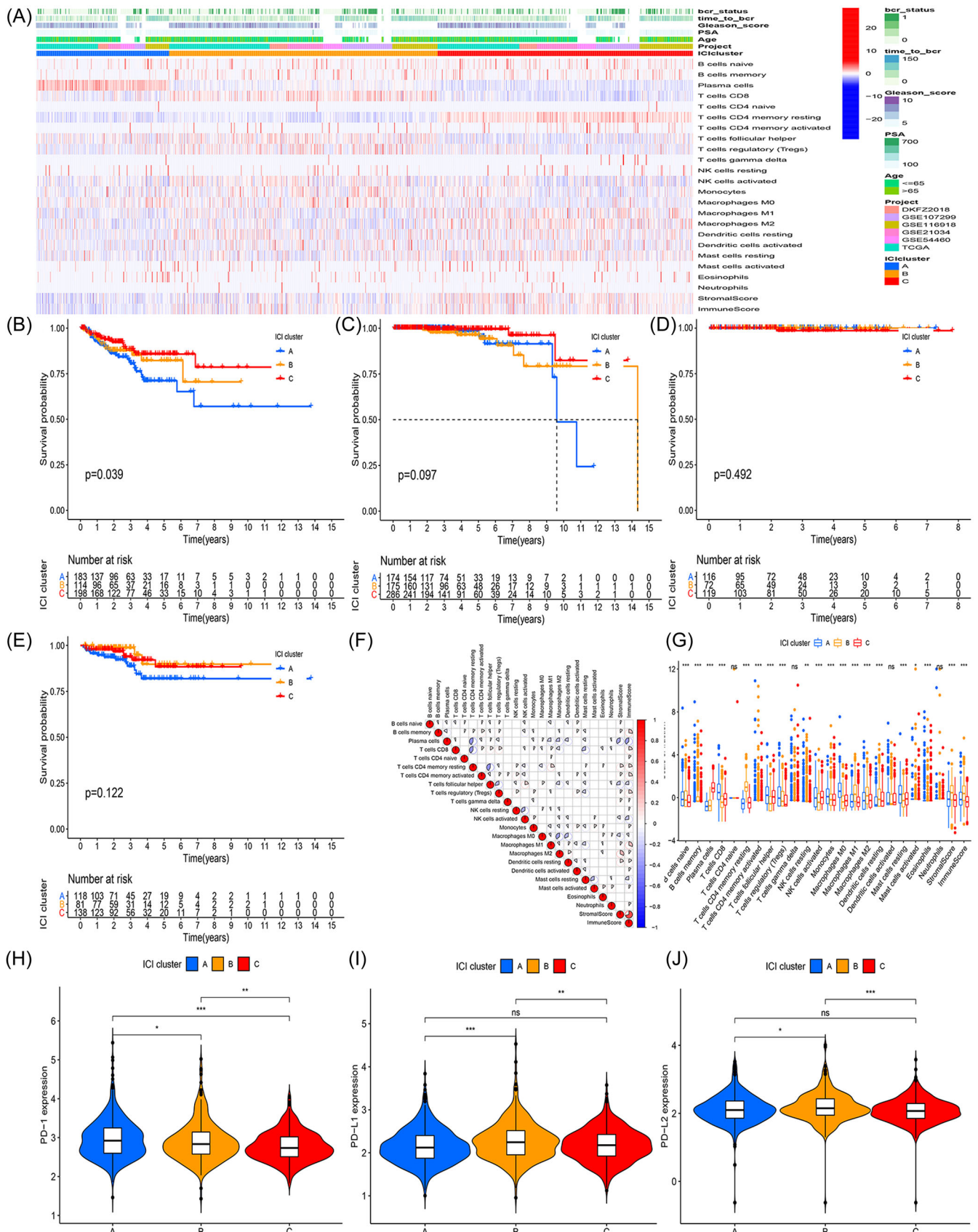


FIGURE 1 (See caption on next page).

To identify statistically significant changes in immune cells and PD1/PD-L1/PD-L2 expression levels among the three ICI subtypes, the Kruskal-Wallis test was used. PD1/PD-L1 expression was significantly elevated in ICI cluster A, while PD1/PD-L1/PD-L2 expression was substantially reduced in ICI cluster C (Figure 1H–J).

3.2 | Recognition of immune gene clusters

Differentially expressed analysis was used to find the transcriptome variance across these subtypes using the limma package of the R program, which shed light on the underlying biology of the various immunophenotypes. The 1405 DEGs were identified (Table S1). Next, the unsupervised clustering approach was performed to investigate the 1405 DEGs, and two genomic clusters, gene clusters A and B, were discovered in the TCGA PCa cohort. The 1273 genes that were shown to have a favorable association with gene clusters were given the designation of ICI gene feature A, whereas the 132 genes were given the designation of ICI gene feature B (Table S2). Additionally, we employed the Boruta approach to reduce the size of ICI gene signatures A and B to eliminate unnecessary or extraneous genes. The 300 DEGs found in the two genomic clusters with the highest abundances were shown in a heat map along with their transcriptome profiles (Figure 2A).

The two genomic clusters were compared using Kaplan-Meier survival analysis, and the difference in survival time's significance was examined using the log-rank test. According to our research, individuals who have The gene cluster A were associated with a better outcome, but those who possessed the gene cluster B had a worse prognosis for PFI (log-rank test, $p < 0.001$; Figure 2B). Gene cluster A was observed in immune-enriched GO terms, including negative regulation of immune system processes, T cell activation, leukocyte proliferation, and leukocyte cell-cell adhesion, as shown in Figure 2C and D and Table S3, Gene cluster B was enriched in cell fate specification, neuronal cell body, neuronal cell body membrane, cation channel activity, and neuropeptide hormone activity. Gene cluster A had high fractions of plasmablasts, CD8 + T cells, T follicular helper cells, Regulatory T cells (Tregs), Monocytes, and Monocyte-derived macrophages (M0 Macrophages). Gene cluster B was enriched by resting memory CD4 + T cells, M1 macrophages, M2 macrophages, Resting dendritic cells, Resting mast cells, Stromal score, and Immune score (Figure 2E). The immune score in gene cluster B was significantly higher in four datasets, while Stromal

Signature and Tumor Purification were relatively higher in gene cluster A.

We performed a Person correlation analysis between ICI signature genes and PD1/PDL1/PD-L2 expression levels and found that the majority of these genes had a strong relationship with these markers (Table S4). Immunocytes and PD1/PD-L1/PD-L2 expression levels were compared across the two genetic groups using the Kruskal-Wallis test for statistical significance. Expression levels of PD1/PD-L1 were found to be substantially greater in gene cluster B, whereas expression levels of PD1/PD-L1/PD-L2 were found to be significantly lower in gene cluster A (Figure 2F,G,I). The greatest concentration of immune cells and stromal cells was found in cluster B of genes, whereas the greatest concentration of tumor cells was found in cluster A of genes. In conclusion, Our categorization system is scientific and fair since the immunological profile and prognosis profile are consistent across gene clusters.

3.3 | Establishment of the ICI score

We utilized principal component analysis (PCA) to construct two total scores to produce a quantitative indication of PCa patients' ICI status: (1) ICI score A for ICI signature gene A; (2) ICI score B for ICI signature gene B. The ICI score A B was calculated separately for each patient in this study and was used as the total of relevant individual scores. Finally, the ICI score was developed as a predictive marker score. Using the best critical values, patients in the meta-cohort were divided into two groups with high or low ICI scores. Figure 3A depicts the patient distribution across the three gene groups. After identifying the usefulness of ICI scores within the TCGA cohort, we next analyzed the immunological activity and tolerance conditions present within each group within the TCGA cohort. CD274, CTLA4, HAVCR2, IDO1, LAG3, and PDCD1 were classified as signatures associated with immunological checkpoints, whereas CD8A, CXCL10, CXCL9, GZMA, GZMB, IFNG, PRF1, TBX2, and TNF were classified as signatures associated with immune activation. Except for LAG3 and PDCD1, the Wilcoxon test revealed that the majority of immune checkpoint and immunological activity-related genes were substantially overexpressed in the high ICI group (Figure 3B). Ribosomal and Oxidative Phosphorylation Pathway were significantly detected by gene set enrichment analysis (GSEA) in the low ICI score group, whereas the high ICI group was enhanced by the Toll-like receptor signaling pathway, B-cell receptor signaling pathway, Natural killer cell-mediated cytotoxicity, JAK-STAT signaling

FIGURE 1 The Landscape of Immunogenomic profiling in the TME of PCa. (A) Hierarchical clustering of tumor-infiltrating immune cells in six independent PCa cohorts. The row represents the tumor-infiltrating immune cells, and the row represents the sample. (B–E) The Kaplan-Meier curve for PFI (B), OS (C), DFI (D), and DSS (E) in meta-cohort with immune cell infiltration. The log-rank test showed a P value less than 0.05. (F) The proportion of immune cells infiltrating the tumor in the three ICI clusters. We also plotted the immune score and stromal score of the three ICI clusters. The Kruskal-Wallis test was used to compare the statistical difference between three ICI clusters. * $p < 0.05$; ** $p < 0.01$; *** $p < 0.001$; **** $p < 0.0001$. (G) Cellular interaction of the tumor-infiltrating immune cell types. (H and I, J) Differences in PD-L1 (H) and PD1 (I), PD-L2 (J) expression between different ICI clusters (Kruskal-Wallis test, $p < 0.0001$).

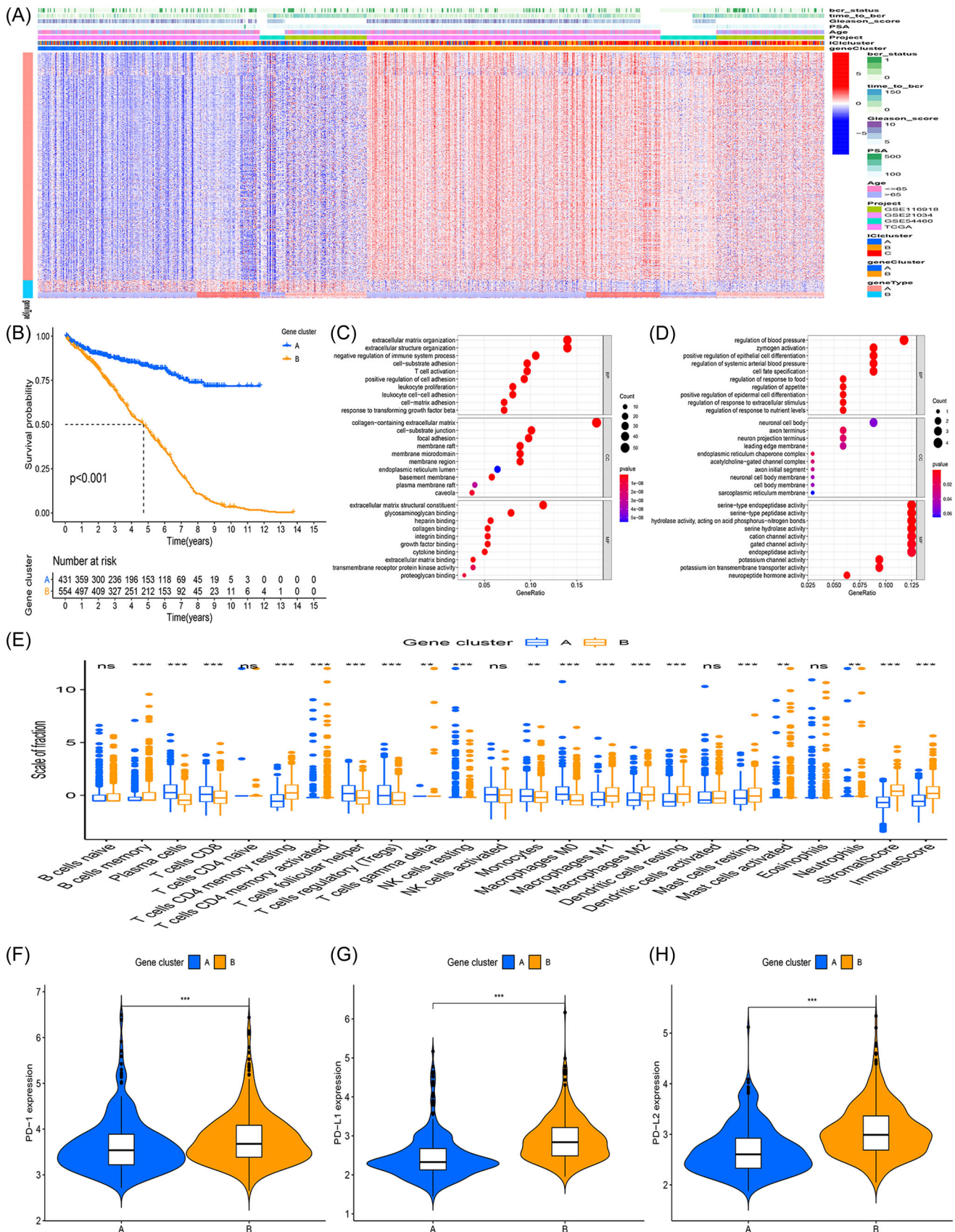


FIGURE 2 (See caption on next page).

pathway, and B-cell receptor signaling pathway (Figure 3C and D; Table S5).

Patients with high ICI scores had considerably lower PFI rates than those with low ICI scores in the merging data, according to the Kaplan-Meier plotter (log-rank test, $p < 0.05$; Figure 3E), GSE116918 (log-rank test, $p < 0.05$; Figure 3F), GSE107299 (log-rank test, $p < 0.05$; Figure 3G), DKF2018 (log-rank test, $p < 0.05$; Figure 3H), Taylor data set (log-rank test, $p < 0.05$; Figure 3I), but not in the TCGA PCa data set (Figure 3J). The findings of the Univariate and Multivariate Cox Regression Analysis also suggest that the ICI score was an independent predictive predictor for PFI (Figure S3A,B).

3.4 | Relationship between ICI scores and somatic mutations

Tumor mutation burden (TMB) is an independent biomarker of ICI response, except for PD-L1 expression.^{14,31} TMB is linked to immunotherapy response in a variety of tumor types and treatment methods, including Checkpoint blockade immunotherapy and cellular therapy.^{31,32} TMB is a measurement of mutations in a tumor and is an important genomic marker that is closely linked to Immunomodulatory therapy and survival prognosis.^{33,34} Given the clinical significance of TMB, we intended to investigate the inherent link between TMB and ICI scores to determine the genetic imprint of each ICI subgroup. Figure 4A shows that patients with a high ICI score had a TMB that was much higher than patients with a low ICI score ($p < 0.05$). Meanwhile, correlation analysis revealed an obvious and inverse link between ICI scores and TMB ($R = -0.17$, $p = 0.00017$; Figure 4B). As depicted in Figure 4C,D, we discovered that patients with low TMB had superior PFI compared to those with high TMB ($p < 0.05$). Overall, these findings suggest that the ICI score was linked to TMB and an effective measure of potential predictive factors of immunotherapy response.

Additionally, somatic variations in PCa driver genes were analyzed using the maftools to compare the frequency of occurrence across low and high ICI categories.³⁰ The top 25 mutated genes with the greatest frequency of change were shown (Figure 4E, Table 2). Out of these genes, SPOP, TP53, TTN, KMT2D, FOXA1, MUC16, KMT2C, SYNE1, and ATM exhibited significant differences between the low ICI subgroup and the high ICI subgroup. These discoveries can potentially offer novel

understandings regarding the immune checkpoint inhibitor composition in cancer and the genetic mutations involved in immune checkpoint blockade therapy.

3.5 | The established ICI scores in predicting the effectiveness of clinical features

The link between clinical features and established ICI scores was evaluated. High ICI scores were linked with high PSA/Gleason scores. Stratified survival analysis suggests that ICI scores were linked to survival. Both high ICI and high Gleason scores were linked to significantly different rates of patient survival depending on the ICI score subtype ($p < 0.05$, Figure 5A–D). Among these patients with a Gleason score of more than 7 ($N = 241$), high ICI scores were related to worse survival, similar results were produced among the patients with a Gleason score of less than 7 ($N = 567$). Similar results were detected between the established ICI model and the PSA level (Figure 5E–H). Among these patients with PSA of more than 10 ng/l ($N = 253$), high ICI scores were related to worse survival and similar results were produced among the patients with PSA of less than 10 ng/l ($N = 555$). Based on Figure 5I,J, it was discovered that a higher ICI score is linked with a positive response to treatment in the meta-cohort (CR/PR: $N = 163$; PD/SD: $N = 30$). Meanwhile, Survival analysis by strata showed that the status of primary therapy outcome success correlated with PFI. Among these patients with Partial/Complete response, high ICI scores were related to worse survival (Figure 5K), and similar results were produced among the patients with Stable/Progressive Disease (Figure 5L).

3.6 | Validation of constructed ICI scores in our PCa cohort

Our study²¹ was deemed eligible for inclusion in the testing set. Patients with a high ICI score had a TMB that was significantly greater than those with a low ICI score (Figure 6A). meanwhile, High ICI scores were linked with high PSA(High PSA: $N = 20$; Low PSA: $N = 44$)/Gleason scores (High Gleason: $N = 40$; Low Gleason: $N = 24$)/TNM stage (Figure 6B–D). These findings were lined with the abovementioned results. Due to the lack of survival time in the validated cohort, survival analysis was not conducted.

FIGURE 2 Hierarchical clustering of prostate cancer (PCa) yields two stable subtypes in meta-cohort. (A) Unsupervised clustering of common DEGs between the three ICI clustering groups was performed to classify patients into two groups: gene clusters A and B. (B) Kaplan-Meier curves for the two genomes between PCa patients. The log-rank test showed statistical significance ($p < 0.05$). (C and D) Gene ontology (GO) enrichment analysis of two ICI-related signature genes: ICI signature gene A (C) and B (D). The x-axis indicates the number of genes in each GO term. (E) The proportion of tumor-infiltrating immune cells in the two gene clusters. We also plotted the immune and stromal scores of the two ICI clusters. Statistical differences between the three ICI clusters were compared by the Kruskal-Wallis test. * $p < 0.05$; ** $p < 0.01$; *** $p < 0.001$; **** $p < 0.0001$. (F–H) The difference in PD-L1 (F) and PD1 (G), PD-L2 (H) expression among different ICI gene clusters (Kruskal-Wallis test, $p < 0.0001$). (F and G, I) Differences in PD-L1 (G) and PD1 (H), PD-L2 (I) expression between two gene clusters (Kruskal-Wallis test, $p < 0.0001$).

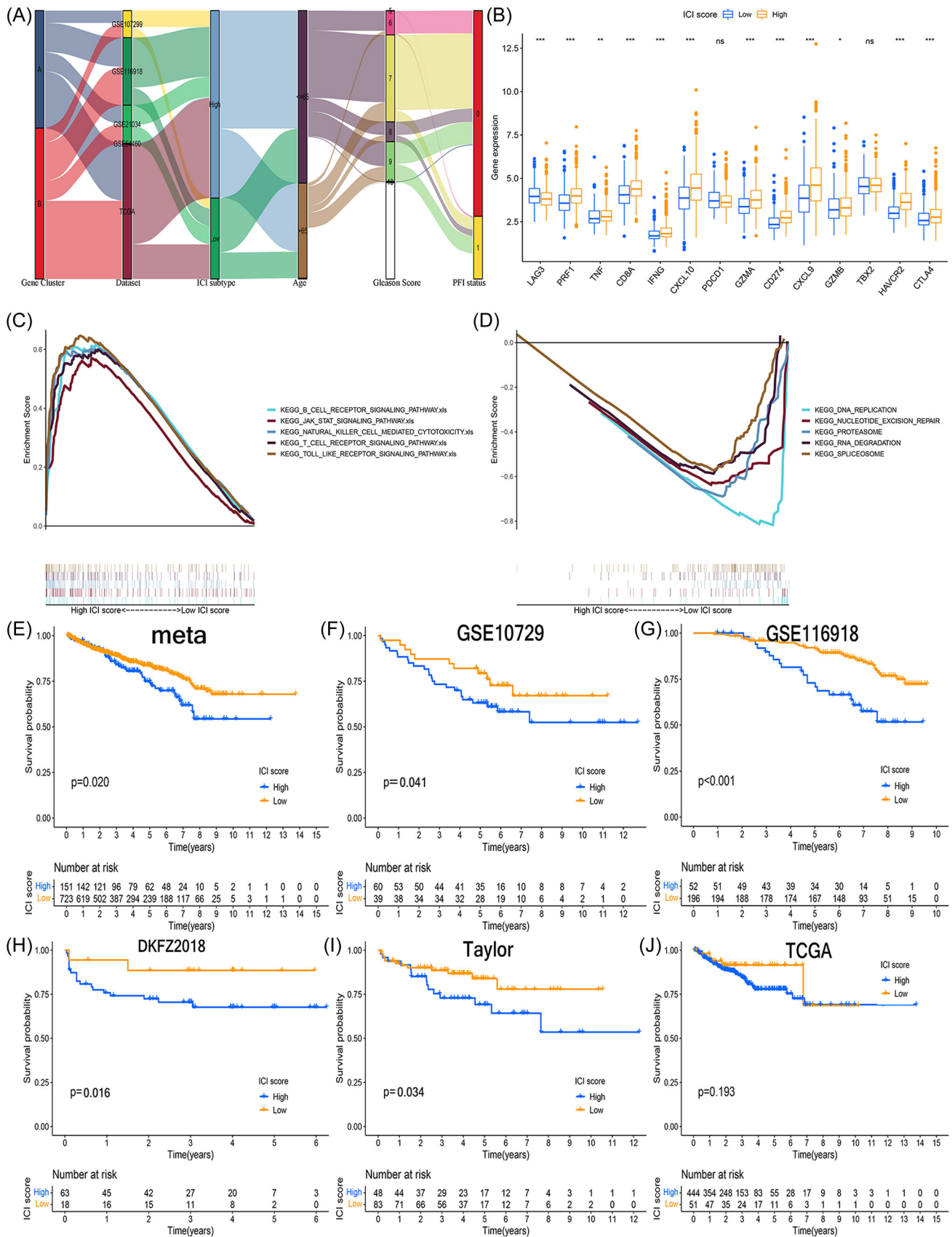


FIGURE 3 (See caption on next page).

4 | DISCUSSION

The TME exerts an essential role in the onset and advancement of cancer. In the complex tumor microenvironment, immune cells such as B-lymphocytes, T-lymphocytes, dendritic cells, macrophages, and others can potentially control cancer development through diverse immune responses. However, the presence of immunosuppressive cells like myeloid-derived suppressor cells (MDSCs), regulatory T cells (Tregs), and tumor-associated macrophages (TAMs) significantly impedes this process. These cells release reactive oxygen species and other inhibitors that suppress the activity of natural killer (NK) cells, which are crucial for targeting and eliminating cancer cells. Additionally, an increased presence of fibroblasts in the tumor environment secretes high levels of metalloproteinases, aiding cancer progression by facilitating the shedding of ligands necessary for NK cell targeting of cancer cells. Fibroblasts also directly inhibit NK cell

function by preventing the upregulation of cytokine-induced activating receptors on NK cells.³⁵ The TME is crucial for Cancer initiation and advancement.^{36,37} The subcategories of memory T cells consist of CD4+ and CD8+ memory T cells, CD8+ memory T cells can eliminate cancerous cells via the secondary identification of tumor-associated antigens. The expansion of T cells is stimulated by CD4+ memory T cells, which in turn hinder the proliferation of tumor cells.³⁸ Growing bodies of research indicate that the activation of CD4 memory T cells is linked to favorable outcomes, as demonstrated in various malignancies including pancreatic adenocarcinoma, prostate cancer, cervical cancer, and non-small cell lung cancer.^{39,40} A major hurdle for effective cancer immunotherapy is an immunosuppressive tumor microenvironment. Cancer immunotherapy has significantly shifted the paradigm of cancer treatment. Focusing on genetic aberrations, CDK12-specific focal tandem duplications can alter the expression levels of oncogenic drivers such as CCND1 and

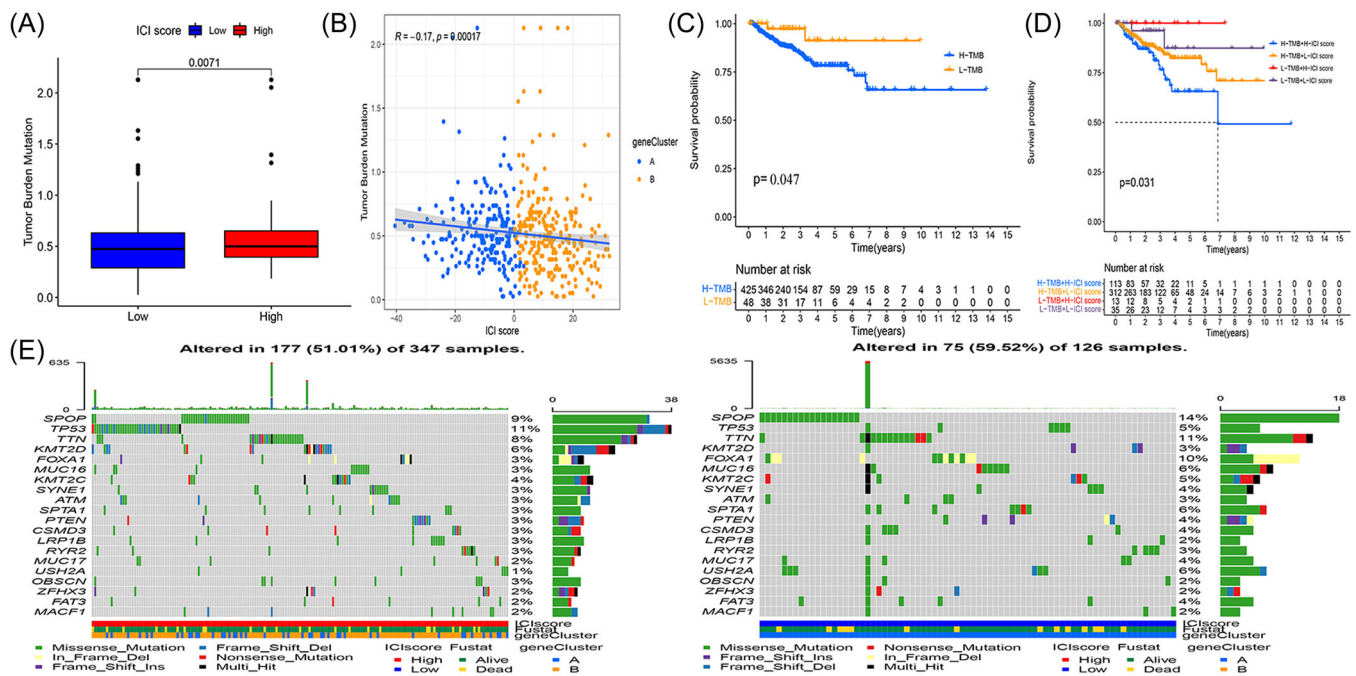


FIGURE 4 Correlation between ICI scores and Somatic mutation. (A) The difference of TMB between high and low ICI score groups (Wilcoxon test, $p = 0.0071$). (B) Scatter plots describe the positive correlation between the ICI scores and the mutation load in the meta-cohort. The Spearman correlation between ICI score and mutation load was exhibited ($p = 0.00017$). (C, D) The Kaplan-Meier curve of the high TMB group and the low TMB group in the meta cohort (Log-rank test, $p = 0.0043$). (E) The oncoPrint was constructed using high ICI scores on the left and low ICI scores on the right. Individual patients are represented in each column.

FIGURE 3 Establishment of ICI score model. (A) Alluvial diagram of ICI gene cluster distribution in groups with different ICI clusters, ICI scores, and survival outcomes. (B) Immune-checkpoint-relevant genes (IDO1, CD274, HAVCR2, PDCD1, CTLA4, and LAG3) and immune-activation-relevant genes (CD8A, CXCL10, CXCL9, GZM A, GZMB, PRF1, IFNG, TBX2, and TNF) expressed in high and low ICI score subgroups. (C) Enrichment plots showing DNA replication, Nucleotide excision repair, Proteasome, RNA degradation, and Spliceosome pathway in the low ICI score subgroup. (D) Enrichment plots showing B cell receptor signaling pathway, JAK stat signaling pathway, Natural killer cell-mediated cytotoxicity, T cell receptor signaling pathway, and Toll-like receptor signaling pathway in the high ICI score subgroup. (E–J) Kaplan-Meier curves of PFI for high and low ICI score groups in the meta cohort (E), DKFZ 2018 cohort (F), Taylor cohort (G), GSE107299 (H), GSE116918 (I), and TCGA Pca cohort (J). Log-rank test, $p < 0.05$ was defined as statistically significant.

TABLE 2 Relationship between ICI score and somatic variation.

Gene	H-wild	H-mutation	L-wild	L-mutation	p value
FOXA1	337(97.12%)	10(2.88%)	114(90.48%)	12(9.52%)	0.005346
NELL1	347(100%)	0(0%)	122(96.83%)	4(3.17%)	0.005689
CDH12	347(100%)	0(0%)	122(96.83%)	4(3.17%)	0.005689
OR6K2	347(100%)	0(0%)	122(96.83%)	4(3.17%)	0.005689
GAD2	347(100%)	0(0%)	122(96.83%)	4(3.17%)	0.005689
APOB	346(99.71%)	1(0.29%)	121(96.03%)	5(3.97%)	0.007
PCDH15	345(99.42%)	2(0.58%)	121(96.03%)	5(3.97%)	0.023206
NWD1	347(100%)	0(0%)	123(97.62%)	3(2.38%)	0.025853
NXN	347(100%)	0(0%)	123(97.62%)	3(2.38%)	0.025853
PCDHGA8	347(100%)	0(0%)	123(97.62%)	3(2.38%)	0.025853
C19orf47	347(100%)	0(0%)	123(97.62%)	3(2.38%)	0.025853
VARS	347(100%)	0(0%)	123(97.62%)	3(2.38%)	0.025853
ARHGEF5	347(100%)	0(0%)	123(97.62%)	3(2.38%)	0.025853
SNX17	347(100%)	0(0%)	123(97.62%)	3(2.38%)	0.025853
LRRC4C	347(100%)	0(0%)	123(97.62%)	3(2.38%)	0.025853
ZNF106	347(100%)	0(0%)	123(97.62%)	3(2.38%)	0.025853
EGF	347(100%)	0(0%)	123(97.62%)	3(2.38%)	0.025853
PTPRN	347(100%)	0(0%)	123(97.62%)	3(2.38%)	0.025853
CNTNAP1	347(100%)	0(0%)	123(97.62%)	3(2.38%)	0.025853
ZNF326	347(100%)	0(0%)	123(97.62%)	3(2.38%)	0.025853
RFC3	347(100%)	0(0%)	123(97.62%)	3(2.38%)	0.025853
EXT1	347(100%)	0(0%)	123(97.62%)	3(2.38%)	0.025853
SPTBN4	347(100%)	0(0%)	123(97.62%)	3(2.38%)	0.025853
ATG2A	347(100%)	0(0%)	123(97.62%)	3(2.38%)	0.025853
SMCHD1	347(100%)	0(0%)	123(97.62%)	3(2.38%)	0.025853
USP12	347(100%)	0(0%)	123(97.62%)	3(2.38%)	0.025853
CLASP1	347(100%)	0(0%)	123(97.62%)	3(2.38%)	0.025853
KIN	347(100%)	0(0%)	123(97.62%)	3(2.38%)	0.025853
NID1	347(100%)	0(0%)	123(97.62%)	3(2.38%)	0.025853
ZNF746	347(100%)	0(0%)	123(97.62%)	3(2.38%)	0.025853
CENPJ	347(100%)	0(0%)	123(97.62%)	3(2.38%)	0.025853
ZMYM4	347(100%)	0(0%)	123(97.62%)	3(2.38%)	0.025853
ARID5B	347(100%)	0(0%)	123(97.62%)	3(2.38%)	0.025853
NOX3	347(100%)	0(0%)	123(97.62%)	3(2.38%)	0.025853
CHRNA10	347(100%)	0(0%)	123(97.62%)	3(2.38%)	0.025853
XPNPEP2	347(100%)	0(0%)	123(97.62%)	3(2.38%)	0.025853
FHOD1	347(100%)	0(0%)	123(97.62%)	3(2.38%)	0.025853
CYP4Z1	347(100%)	0(0%)	123(97.62%)	3(2.38%)	0.025853
SLC6A5	347(100%)	0(0%)	123(97.62%)	3(2.38%)	0.025853

TABLE 2 (Continued)

Gene	H-wild	H-mutation	L-wild	L-mutation	p value
ACACA	346(99.71%)	1(0.29%)	122(96.83%)	4(3.17%)	0.027454
TIAM2	346(99.71%)	1(0.29%)	122(96.83%)	4(3.17%)	0.027454
THSD7B	346(99.71%)	1(0.29%)	122(96.83%)	4(3.17%)	0.027454
VPS13B	346(99.71%)	1(0.29%)	122(96.83%)	4(3.17%)	0.027454
PLAA	346(99.71%)	1(0.29%)	122(96.83%)	4(3.17%)	0.027454
SCN5A	346(99.71%)	1(0.29%)	122(96.83%)	4(3.17%)	0.027454
GPR158	346(99.71%)	1(0.29%)	122(96.83%)	4(3.17%)	0.027454
PTPRC	346(99.71%)	1(0.29%)	122(96.83%)	4(3.17%)	0.027454
USH2A	342(98.56%)	5(1.44%)	119(94.44%)	7(5.56%)	0.028886

Note: The p values of different ICI subtypes were tested by the chi-square test.

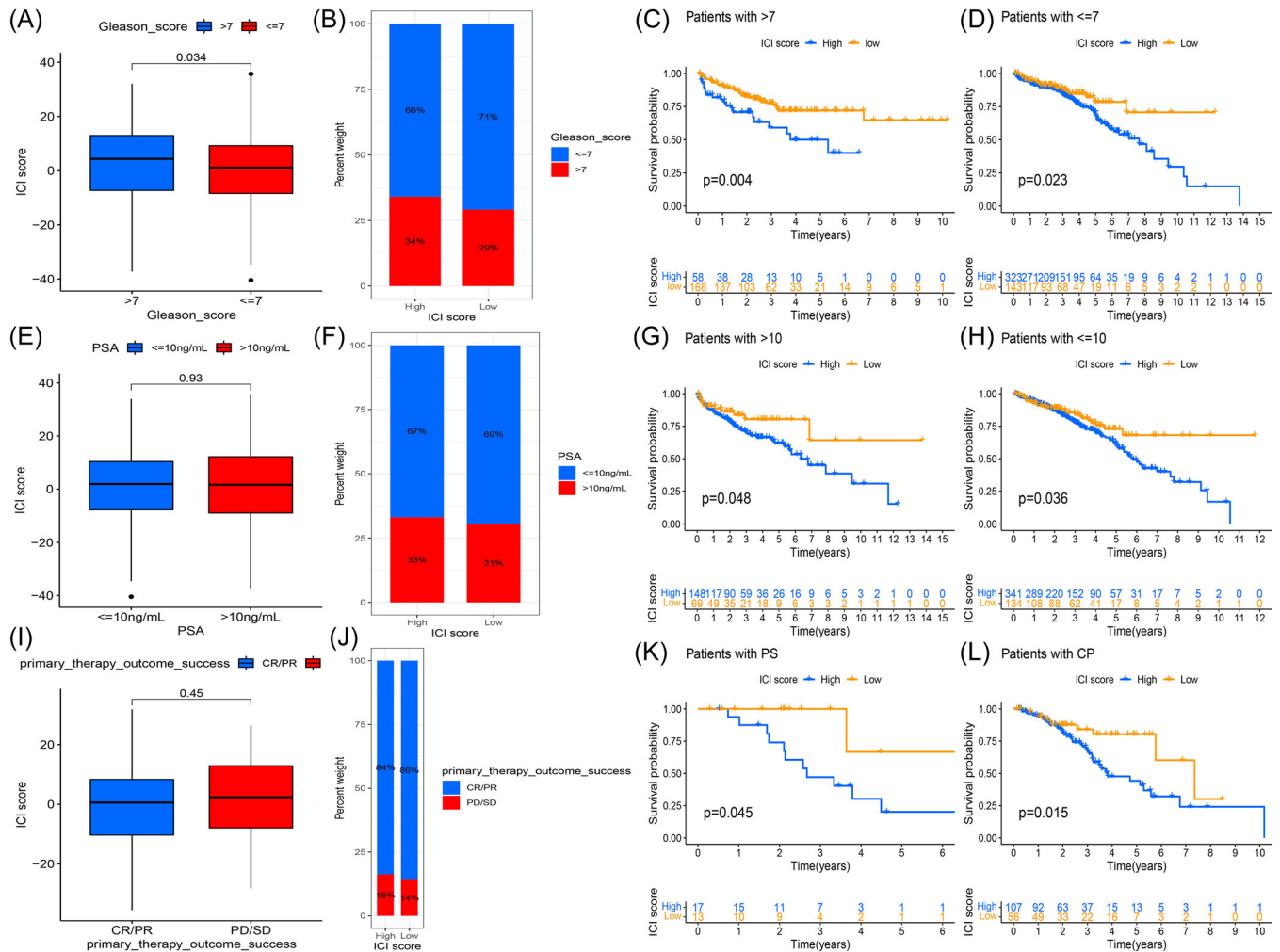


FIGURE 5 The ICI Scores correlated with clinical features. (A and B, C, D) ICI scores in groups with different Gleason (A, B)/PSA scores (C, D). Wilcox on test, $p < 0.0001$. (E-H) Stratified survival analysis showed that ICI scores were associated with survival. Kaplan-Meier curves for patients with high and low ICI scores and different Gleason (E, F)/PSA scores (G, H) in the meta cohort. Log-rank test, $P < 0.05$. (I, J) ICI scores in groups with a different clinical response status. (K, L) Kaplan-Meier curves for patients with high and low ICI scores in the TCGA PCa cohort.

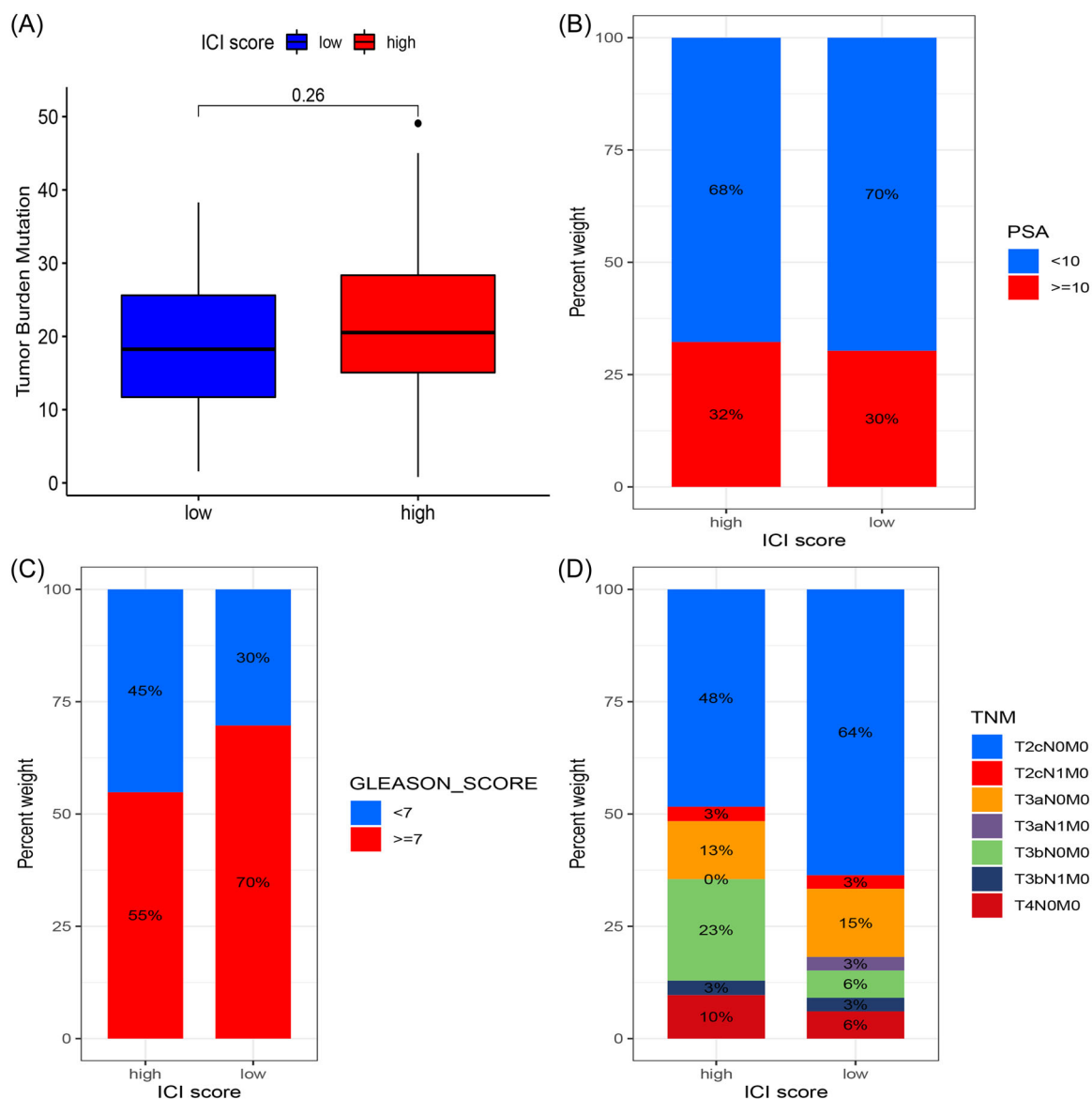


FIGURE 6 Validation of ICI scores in our PCa cohort. (A) The box plot exhibited the distribution of TNM between high and low ICI groups. (B–D) ICI scores in groups with different PSA (B), Gleason (C), and TNM stage (D).

CDK4. This alteration suggests a potential vulnerability of CDK12-mutated tumors to CDK4/6 inhibitors. Additionally, the presence of CDK12 aberrations, alongside mismatch repair deficiency, can serve as a biomarker for predicting treatment responses. This understanding underpins ongoing clinical trials exploring the combined use of immune checkpoint blockade and CDK4/6 inhibition as a promising therapeutic strategy for cancer.⁴¹ Cancer immunotherapy has demonstrated lasting clinical benefits in patients with cancer.^{42,43} Several studies reported that immunosuppressive therapy is most effective in eradicating tumor-causing growth and can improve the quality of life of patients with recurring or metastatic PCa.^{44–46} However, immunotherapy is now a part of the armamentarium for prostate cancer, but there remains room for improvement.⁴⁴ One major drawback of immunosuppressive treatment is that it has only been tried out on a limited number of people.⁴⁷

Although several studies have demonstrated that TME was involved in the occurrence of head and neck squamous cell carcinoma,⁴⁸ hepatocellular carcinoma,⁴⁹ and ovarian cancer³⁹ using public datasets, these studies failed to validate these results in another data set. In this study, we established a method to quantify the full tumor immune environment in PCa and validated the findings in another data set. Our findings suggest that the ICI score is a reliable predictor and prognostic biomarker for assessing response to immunosuppressive treatment.

More and more pieces of evidence demonstrated that Immune suppression is facilitated by immune cell malfunction in PCa-TME, which is related to tumor survival and progression. In this work, we looked at ICIs from a meta-analysis of 1341 PCa samples and divided them into three immunological subgroups. Our findings support earlier research suggesting CD4+ helper T cells, dendritic cells,

plasma cells, M1 polarized macrophages, M2 polarized macrophages, and a higher immunological score is connected with patient prognosis.^{50,51} In the work, ICI cluster C has a higher abundance of macrophage M2 and a better prognosis, which is controversial in previous studies.^{52,53} We speculated the reason is that the CIBERSORT method itself is developed based on microarray data, and sequencing data may not always be appropriate. Multiple research works have identified prostate cancer as an immunogenic disorder, thereby emphasizing the prudent considerations of immune cell function in the tumor-associated microenvironment during tumor progression.^{54,55} Currently, the precise contribution of immune cells in the tumor microenvironment toward the pathogenesis of cancer, particularly in the context of prostate cancer, remains incompletely understood. While immunosuppressive therapy has shown effectiveness in managing malignancies such as melanoma, its application in prostate cancer has not yet demonstrated similar significant therapeutic potential. In this context, it is pertinent to note that patients with melanoma of unknown primary (MUP) often experience better outcomes compared to those with stage-matched known primary melanoma (MKP). This difference is likely attributable to the higher immunogenicity observed in MUP, which may induce an immunologically mediated regression of the primary tumor site. Such observations highlight the varying responses to immunotherapy across different types of malignancies and underscore the need for further research in this area.⁵⁶ Immunosuppressive therapy is effective in less than 20% of prostate cancer patients when compared with other tumors displaying lower levels of immune dysfunction.⁵⁷ This suggests that the immune phenotype in tumors is also not an absolute predictor of immunotherapeutic response. We speculate that these molecular changes during tumor formation may disturb cell-to-cell communication among immune cells that are filtering, thereby causing an imbalance in immune tolerance and activity.

In this study, we postulated that developing personalized treatment strategies for individual patients could be facilitated by the concurrent analysis of the ICI subgroup and immune-related gene expression patterns. Our primary focus is on identifying the molecular features of PCa-TME that modulate the immune response. To achieve this, we first identified immune-related genes utilizing the recently proposed ICI gene cluster. Among these gene clusters, our analysis revealed that ICI gene cluster B exhibited elevated scores in terms of immune response-related parameters such as immune scores, matrix scores, as well as other cell types involved in the immune response. These results suggest the presence of an immune-cold phenotype. On the contrary, ICI gene cluster A exhibited a lower immune score and a greater abundance of inflammatory cells. Besides, we observed that high matrix scores were linked to a higher infiltration of TAM and increased resting/activated DCs in ICI gene cluster B, suggesting an antibody-based immune response in this cluster. Moreover, ICI gene cluster A exhibited a more advantageous immune-activated phenotype with the highest concentration of CD8+ T cells, activated follicular helper T cells, regulatory T cells (Tregs), and

antibody-secreting plasma cells. A tumor-suppressive immune response was linked to a favorable outlook and increased ICI scores in ICI gene cluster B. In contrast, we posited that patients within ICI gene cluster A might reap the benefits of immunotherapy, given the immune-activated phenotype observed within this cluster, while a lack of immune activity within this cluster was correlated with a worse prognosis.

To summarize, we have thoroughly investigated the ICI profile of PCa to obtain a comprehensive understanding of its impact on regulating antitumor immune responses. Our analysis revealed that differences in ICI patterns were linked to tumor heterogeneity and therapeutic complexities, underscoring the clinical significance of the systematic appraisal of tumor ICI patterns. Moreover, this can aid in identifying optimal candidates for targeted immunotherapeutic interventions.

AUTHOR CONTRIBUTIONS

J.K.S; Y.D.W; X.H.Y wrote the main manuscript text; J.K.S; Y.D.W prepared Figures 1–6; J.K.S contributed to data analysis; All authors reviewed the manuscript. The corresponding author has full access to all data in this study and assumes full responsibility for the completeness and accuracy of data analysis.

ACKNOWLEDGMENTS

This project was supported by Supported by Guizhou Provincial Basic Research Program (Natural Science) (No. Qian Ke He Basic-ZK (2021) General 377) and Science and Technology Fund of Guizhou Provincial Health Commission (NO. gzwjkj2019-1-130).

CONFLICT OF INTEREST STATEMENT

The authors declare no conflict of interest. **Guarantor:** J.K.S was the guarantor.

DATA AVAILABILITY STATEMENT

The data that support the findings of this study are available in TCGA at <https://portal.gdc.cancer.gov/>. These data were derived from the following resources available in the public domain: - geo, <https://www.ncbi.nlm.nih.gov/geo/>. Data availability could be obtained from TCGA and GEO websites. The corresponding author, Jukun Song confirms that this manuscript is an honest, accurate, and transparent explanation of the reported research. No important aspects of the research were overlooked. Explained any differences between the planned and registered studies.

TRANSPARENCY STATEMENT

The lead author Jukun Song affirms that this manuscript is an honest, accurate, and transparent account of the study being reported; that no important aspects of the study have been omitted; and that any discrepancies from the study as planned (and, if relevant, registered) have been explained.

ORCID

Jukun Song  <http://orcid.org/0000-0003-2542-9340>

REFERENCES

- Siegel RL, Miller KD, Jemal A. Cancer statistics, 2020. *CA Cancer J Clin.* 2020;70:7-30.
- Jemal A, Bray F, Center MM, Ferlay J, Ward E, Forman D. Global cancer statistics. *CA Cancer J Clin.* 2011;61:69-90.
- Talkar SS, Patravale VB. Gene therapy for prostate cancer: a review. *Endocr Metab Immune Disord Drug Targets.* 2021;21:385-396.
- Evans AJ. Treatment effects in prostate cancer. *Mod Pathol.* 2018;31:110-121.
- Van den Broeck T, van den Bergh RCN, Arfi N, et al. Prognostic value of biochemical recurrence following treatment with curative intent for prostate cancer: a systematic review. *Eur Urol.* 2019;75:967-987.
- Bernard B, Sweeney CJ. Management of metastatic hormone-sensitive prostate cancer. *Curr Urol Rep.* 2015;16:14.
- Attard G, Murphy L, Clarke NW, et al. Abiraterone acetate plus prednisolone with or without enzalutamide for patients with metastatic prostate cancer starting androgen deprivation therapy: final results from two randomised phase 3 trials of the STAMPEDE platform protocol. *Lancet Oncol.* 2023;24:443-456.
- Saxby H, Mikropoulos C, Boussios S. An update on the prognostic and predictive serum biomarkers in metastatic prostate cancer. *Diagnostics.* 2020;10:549.
- Arce M, Pinto MP, Galleguillos M, et al. Coagulation factor Xa promotes solid tumor growth, experimental metastasis and endothelial cell activation. *Cancers.* 2019;11:1103.
- Brepmpelis KJ, Cowan CM, Kreuser SA, et al. Genetically engineered macrophages persist in solid tumors and locally deliver therapeutic proteins to activate immune responses. *J Immunother Cancer.* 2020;8:e001356.
- Kather JN, Hörner C, Weis CA, et al. CD163+ immune cell infiltrates and presence of CD54+ microvessels are prognostic markers for patients with embryonal rhabdomyosarcoma. *Sci Rep.* 2019;9:9211.
- Mandal A, Viswanathan C. Natural killer cells: in health and disease. *Hematol Oncol Stem Cell Ther.* 2015;8:47-55.
- Wang F, Wang S, Zhou Q. The resistance mechanisms of lung cancer immunotherapy. *Front Oncol.* 2020;10:568059.
- Seiwert TY, Burtneß B, Mehra R, et al. Safety and clinical activity of pembrolizumab for treatment of recurrent or metastatic squamous cell carcinoma of the head and neck (KEYNOTE-012): an open-label, multicentre, phase 1b trial. *Lancet Oncol.* 2016;17:956-965.
- Hamid O, Robert C, Daud A, et al. Safety and tumor responses with lambrolizumab (anti-PD-1) in melanoma. *N Engl J Med.* 2013;369:134-144.
- Long Q, Xu J, Osunkoya AO, et al. Global transcriptome analysis of formalin-fixed prostate cancer specimens identifies biomarkers of disease recurrence. *Cancer Res.* 2014;74:3228-3237.
- Sinha A, Huang V, Livingstone J, et al. The proteogenomic landscape of curable prostate cancer. *Cancer Cell.* 2019;35:414-427.e6.
- Jain S, Lyons CA, Walker SM, et al. Validation of a metastatic assay using biopsies to improve risk stratification in patients with prostate cancer treated with radical radiation therapy. *Ann Oncol.* 2018;29:215-222.
- Taylor BS, Schultz N, Hieronymus H, et al. Integrative genomic profiling of human prostate cancer. *Cancer Cell.* 2010;18:11-22.
- Gerhauser C, Favero F, Risch T, et al. Molecular evolution of early-onset prostate cancer identifies molecular risk markers and clinical trajectories. *Cancer Cell.* 2018;34:996-1011.e8.
- Ren S, Wei GH, Liu D, et al. Whole-genome and transcriptome sequencing of prostate cancer identify new genetic alterations driving disease progression. *Eur Urol.* 2018;73:322-339.
- Davis S, Meltzer PS. GEOquery: a bridge between the Gene Expression Omnibus (GEO) and BioConductor. *Bioinformatics.* 2007;23:1846-1847.
- Cerami E, Gao J, Dogrusoz U, et al. The cBio cancer genomics portal: an open platform for exploring multidimensional cancer genomics data. *Cancer Discovery.* 2012;2:401-404.
- Johnson WE, Li C, Rabinovic A. Adjusting batch effects in microarray expression data using empirical Bayes methods. *Biostatistics.* 2007;8:118-127.
- Newman AM, Liu CL, Green MR, et al. Robust enumeration of cell subsets from tissue expression profiles. *Nat Methods.* 2015;12:453-457.
- Yoshihara K, Shahmoradgoli M, Martínez E, et al. Inferring tumour purity and stromal and immune cell admixture from expression data. *Nat Commun.* 2013;4:2612.
- Wilkerson MD, Hayes DN. ConsensusClusterPlus: a class discovery tool with confidence assessments and item tracking. *Bioinformatics.* 2010;26:1572-1573.
- Ritchie ME, Phipson B, Wu D, et al. limma powers differential expression analyses for RNA-seq and microarray studies. *Nucleic Acids Res.* 2015;43:e47.
- Speiser JL, Miller ME, Tooze J, Ip E. A comparison of random forest variable selection methods for classification prediction modeling. *Expert Syst Appl.* 2019;134:93-101.
- Mayakonda A, Lin DC, Assenov Y, Plass C, Koeffler HP. Maftools: efficient and comprehensive analysis of somatic variants in cancer. *Genome Res.* 2018;28:1747-1756.
- Cristescu R, Mogg R, Ayers M, et al. Pan-tumor genomic biomarkers for PD-1 checkpoint blockade-based immunotherapy. *Science.* 2018;362:eaar3593.
- Danaher P, Warren S, Lu R, et al. Pan-cancer adaptive immune resistance as defined by the Tumor Inflammation Signature (TIS): results from The Cancer Genome Atlas (TCGA). *J Immunother Cancer.* 2018;6:63.
- Hatakeyama K, Nagashima T, Ohshima K, et al. Mutational burden and signatures in 4000 Japanese cancers provide insights into tumorigenesis and response to therapy. *Cancer Sci.* 2019;110:2620-2628.
- McGray AJR, Huang RY, Battaglia S, et al. Oncolytic Maraba virus armed with tumor antigen boosts vaccine priming and reveals diverse therapeutic response patterns when combined with checkpoint blockade in ovarian cancer. *J Immunother Cancer.* 2019;7:189.
- Das A, Ghose A, Naicker K, et al. Advances in adoptive T-cell therapy for metastatic melanoma. *Curr Res Transl Med.* 2023;71:103404.
- Liu W, Bi S, Li C, et al. Purification and characterization of a new CRISP-related protein from Scapharca broughtonii and its immunomodulatory activity. *Mar Drugs.* 2020;18:299.
- Senaratna CV, Perret JL, Lodge CJ, et al. Prevalence of obstructive sleep apnea in the general population: a systematic review. *Sleep Med Rev.* 2017;34:70-81.
- Liu C, Hu Q, Xu B, et al. Peripheral memory and naïve T cells in non-small cell lung cancer patients with lung metastases undergoing stereotactic body radiotherapy: predictors of early tumor response. *Cancer Cell Int.* 2019;19:121.
- Liu J, Tan Z, He J, et al. Identification of three molecular subtypes based on immune infiltration in ovarian cancer and its prognostic value. *Biosci Rep.* 2020;40:1-17.
- Joyce JA, Fearon DT. T cell exclusion, immune privilege, and the tumor microenvironment. *Science.* 2015;348:74-80.
- Shah S, Rachmat R, Enyoma S, Ghose A, Revythis A, Boussios S. BRCA mutations in prostate cancer: assessment, implications and treatment considerations. *Int J Mol Sci.* 2021;22:12628.
- Pickles OJ, Lee LYW, Starkey T, et al. Immune checkpoint blockade: releasing the breaks or a protective barrier to COVID-19 severe acute respiratory syndrome? *Br J Cancer.* 2020;123:691-693.
- Ajina R, Zamalin D, Weiner LM. Functional genomics: paving the way for more successful cancer immunotherapy. *Briefings Funct Genomics.* 2019;18:86-98.

44. Cha E, Fong L. Immunotherapy for prostate cancer: biology and therapeutic approaches. *J Clin Oncol*. 2011;29:3677-3685.
45. Garcia AJ, Ruscetti M, Arenzana TL, et al. Pten null prostate epithelium promotes localized myeloid-derived suppressor cell expansion and immune suppression during tumor initiation and progression. *Mol Cell Biol*. 2014;34:2017-2028.
46. Zhao L, Fu X, Han X, Yu Y, Ye Y, Gao J. Tumor mutation burden in connection with immune-related survival in uterine corpus endometrial carcinoma. *Cancer Cell Int*. 2021;21:80.
47. Barresi V, Simbolo M, Mafficini A, et al. Ultra-mutation in IDH wild-type glioblastomas of patients younger than 55 years is associated with defective mismatch repair, microsatellite instability, and giant cell enrichment. *Cancers*. 2019;11:1279.
48. Zhang X, Shi M, Chen T, Zhang B. Characterization of the immune cell infiltration landscape in head and neck squamous cell carcinoma to aid immunotherapy. *Mol Ther Nucleic Acids*. 2020;22:298-309.
49. Yang S, Cheng Y, Wang X, Wei P, Wang H, Tan S. Identification of the immune cell infiltration landscape in hepatocellular carcinoma to predict prognosis and guide immunotherapy. *Front Genet*. 2021;12:777931.
50. Rooney MS, Shukla SA, Wu CJ, Getz G, Hacohen N. Molecular and genetic properties of tumors associated with local immune cytolytic activity. *Cell*. 2015;160:48-61.
51. Bousset L, Septier A, Bunay J, et al. Absence of nuclear receptors LXR α impairs immune response to androgen deprivation and leads to prostate neoplasia. *PLoS Biol*. 2020;18:e3000948.
52. Azizi E, Carr AJ, Plitas G, et al. Single-cell map of diverse immune phenotypes in the breast tumor microenvironment. *Cell*. 2018;174:1293-1308.e36.
53. Cortese N, Carriero R, Laghi L, Mantovani A, Marchesi F. Prognostic significance of tumor-associated macrophages: past, present and future. *Sem Immunol*. 2020;48:101408.
54. Bou-Dargham MJ, Sha L, Sang QXA, Zhang J. Immune landscape of human prostate cancer: immune evasion mechanisms and biomarkers for personalized immunotherapy. *BMC Cancer*. 2020;20:572.
55. Song W, Shen L, Wang Y, et al. Synergistic and low adverse effect cancer immunotherapy by immunogenic chemotherapy and locally expressed PD-L1 trap. *Nat Commun*. 2018;9:2237.
56. Boussios S, Rassy E, Samartzis E, et al. Melanoma of unknown primary: new perspectives for an old story. *Crit Rev Oncol Hematol*. 2021;158:103208.
57. Yarchoan M, Hopkins A, Jaffee EM. Tumor mutational burden and response rate to PD-1 inhibition. *N Engl J Med*. 2017;377:2500-2501.

SUPPORTING INFORMATION

Additional supporting information can be found online in the Supporting Information section at the end of this article.

How to cite this article: Yin X, Wu Y, Song J. Characteristics of the immune environment in prostate cancer as an adjunct to immunotherapy. *Health Sci Rep*. 2024;7:e2148. doi:10.1002/hsr2.2148